An Atomistic Study of Interfacial Diffusion in Lamellar TiAl Alloys

M. NOMURA AND V. VITEK

*Department of Materials Science and Engineering, University of Pennsylvania, Philadelphia,
Pennsylvania, 19104-6272, USA*

Abstract.   In this paper we investigate self-diffusion of Ti and Al along interfaces present in the lamellar $L1_0$ TiAl by atomistic computer modeling. The interactions between the atoms are described by centralforce many-body potentials. The approach adopted is similar to that used in earlier atomistic modeling of bulk diffusion in TiAl [1, 2]. Both the formation and migration of vacancies is examined. The interfaces studied are the three types of $\gamma-\gamma$ interfaces: ordinary twin, pseudotwin and $120°$ rotational fault. For the latter two interfaces the diffusion was investigated not only for the stoichiometric case but also when the interfaces possess a surplus of titanium in the form of a layer with the composition and structure of Ti_3Al, as was found in an earlier Monte Carlo study of titanium segregation to these interfaces. The calculations suggest that the diffusivity along $\gamma-\gamma$ interfaces is higher than in the bulk. However, the difference between bulk and interfacial diffusivity is not as drastic as it may be encountered in grain boundaries. At the same time the above mentioned surplus of Ti appears to affect the interfacial diffusion only marginally.

Keywords: diffusion, lamellar interfaces, vacancy, antisite defect, effective formation and migration energy, segregation

1.   Introduction

The appeal of intermetallic compounds to engineers and materials scientists stems from their attractive combination of physical and mechanical properties, in particular exceptionally high strength, hardness, creep and corrosion resistance at high temperatures [3–6]. A negative feature of these materials is frequently their small or even non-existent ductility at ambient temperatures. Yet, in several instances intermetallics that display an acceptable ductility are two-phase materials with coherent interfaces [7]. Titanium-aluminum alloys based on γ-TiAl with the tetragonal $L1_0$ structure belong to this category. Remarkably high plastic strain levels have been achieved under tension at room temperature in the lamellar structure composed of layers of multiply oriented $L1_0$ TiAl interspersed with the hexagonal, DO_{19}, Ti_3Al [6, 8–11]. These compounds are materials of increasing technological importance in high-temperature applications [6, 12–17] and their formation, high-temperature stability, as well as their creep resistance, all depend on or are controlled by diffusion.

Present understanding of diffusion processes in TiAl is far from complete although a significant progress, both experimental and theoretical, has recently been made in studies of bulk diffusion in this compound [1, 2]. It is well known that interfacial and grain boundary diffusion is often much faster than the bulk diffusion [18–24] and thus owing to the lamellar structure a significant fraction of diffusional transport may occur at lamellar interfaces. On the other hand, as explained in more detail below, the $\gamma-\gamma$ lamellar interfaces are twin-like and possess high symmetries and their structures may be highly ordered [25, 26]. Hence, it is not a priori evident that they do represent paths of fast diffusion. Diffusion in $\gamma-\gamma$ lamellar interfaces has not been investigated either experimentally or theoretically and it is the goal of this atomistic study to elucidate the self-diffusion in these interfaces and assess its importance relative to the diffusion in the bulk.

The approach adopted in the present work is similar to that followed by Mishin and Herzig [1, 2] in their theoretical investigation of bulk diffusion in TiAl. Computer simulation, utilizing central-force many body

potentials that are akin to the embedded atom method (EAM) used in [1, 2], is employed to investigate the diffusion process assuming that self-diffusion occurs via the motion of vacancies. Both the formation and migration of vacancies has been examined following the procedures analogous to those employed in [1, 2]. The interfaces studied were the three types of $\gamma-\gamma$ interfaces, described in Section 2; the interface between the $L1_0$ TiAl and the DO_{19} Ti_3Al has not been included into this study. On the other hand, not only stoichiometric $\gamma-\gamma$ interfaces have been considered but also interfaces with surplus of titanium that may occur due to segregation [27, 28]. As suggested in earlier experimental [27] and theoretical studies [28], the structure of such interfaces can be considered as containing a thin layer of Ti_3Al. The results of the present calculations suggest that in all three $\gamma-\gamma$ interfaces both formation and migration energies of vacancies are lower than in the bulk and, therefore, the diffusivity along them is higher. However, the difference between the bulk and interfacial diffusivity is not as drastic as it is found in many grain boundaries. At the same time the above mentioned surplus of Ti appears to affect the interfacial diffusion only marginally.

2. $\gamma-\gamma$ Interfaces in Lamellar TiAl

While the $L1_0$ structure is tetragonal, it is customary to use the cubic notation for planes and directions since this structure can be regarded as fcc based if the c/a ratio is close to 1. In the following the tetragonal c-axis will always be the [001] direction. Using this notation, $L1_0$ TiAl structure can be regarded as alternate (001) layers of Al and Ti atoms (see Fig. 1). In the lamellar TiAl $\gamma-\gamma$ interfaces are all parallel to $\{111\}$ planes and Fig. 2(a) shows the atomic structure of the ideal $L1_0$ lattice in the $[\bar{1}10]$ projection as a stacking of (111) planes.

Since there are six possible relative orientations of the $\langle\bar{1}10\rangle$ or, alternatively, $\langle\bar{1}\bar{1}2\rangle$ vectors in the $\{111\}$ planes of adjacent lamellae, three distinct $\gamma-\gamma$ interfaces may exist [24, 25, 29]: The ordered twin, obtained when $[\bar{1}\bar{1}2]_1$ is parallel to $[11\bar{2}]_u$ (Fig. 2(b)), the pseudotwin when $[\bar{1}\bar{1}2]_1$ is parallel to $[1\bar{2}1]_u$ or $[\bar{2}11]_u$ (Fig. 2(c)), and the 120° rotational fault when $[\bar{1}\bar{1}2]_1$ is parallel to $[\bar{1}2\bar{1}]_u$ or $[2\bar{1}\bar{1}]_u$ (Fig. 2(d)); the subscripts l and u refer to the lower and upper lamella, respectively. In Fig. 2(a)–(d) the interfacial (111) layers in which formation and migration of vacancies has been considered, are marked by numbers.
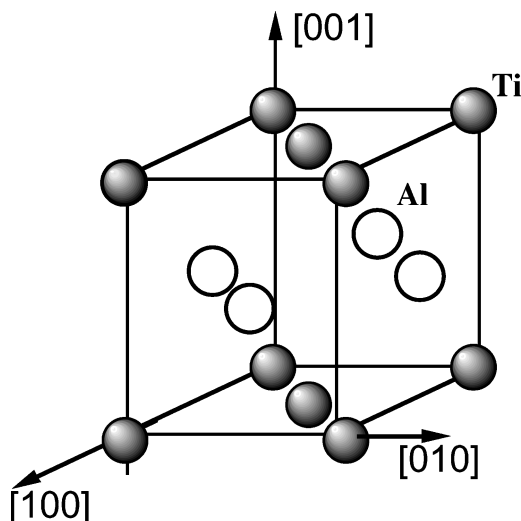
Figure 1.   Unit cell of the $L1_0$ TiAl structure; open circles represent Al and filled circles Ti.

Lamellar titanium-aluminum alloys based on γ-TiAl are generally titanium rich [8, 9, 30] and segregation of Ti to the $\gamma-\gamma$ interfaces defined above is possible. This has, indeed, been corroborated experimentally [27] and results of a recent Monte Carlo study [28] suggest that in Ti-rich alloys a very thin layer with composition close to the DO_{19} Ti_3Al forms at 120° rotational faults and pseudotwins (but not in ordered twins). For this reason we have also investigated formation and migration of vacancies in the 120° rotational fault and the pseudotwin in which the central layer, i.e. layer 0 in Fig. 1(c) and (d), has the composition of Ti_3Al, while all the other layers possess the stoichiometric TiAl composition.

In $L1_0$ TiAl the c/a ratio is 1.017 [31]. This non-ideal c/a ratio does not invoke any misfit at the ordered twin. However, it causes that $[1\bar{2}1]$ and $[\bar{2}11]$ vectors are a factor of 1.0085 shorter than the vector $[\bar{1}\bar{1}2]$, which leads to a misfit at the 120°rotational fault and the pseudotwin. This mismatch is then compensated by a network of misfit dislocations [32]. However, since the misfit is small, the separation of these dislocations is large, of the order of fifty lattice spacings, and periods of these interfaces have the same dimensions. Atomistic modeling of such long-period interfaces would require very large numbers of atoms. Yet, the interfacial regions in between the misfit dislocations are structurally very similar to the short period interfaces that arise for the ideal $c/a = 1$ ratio. Consequently, in the present study we have investigated only short
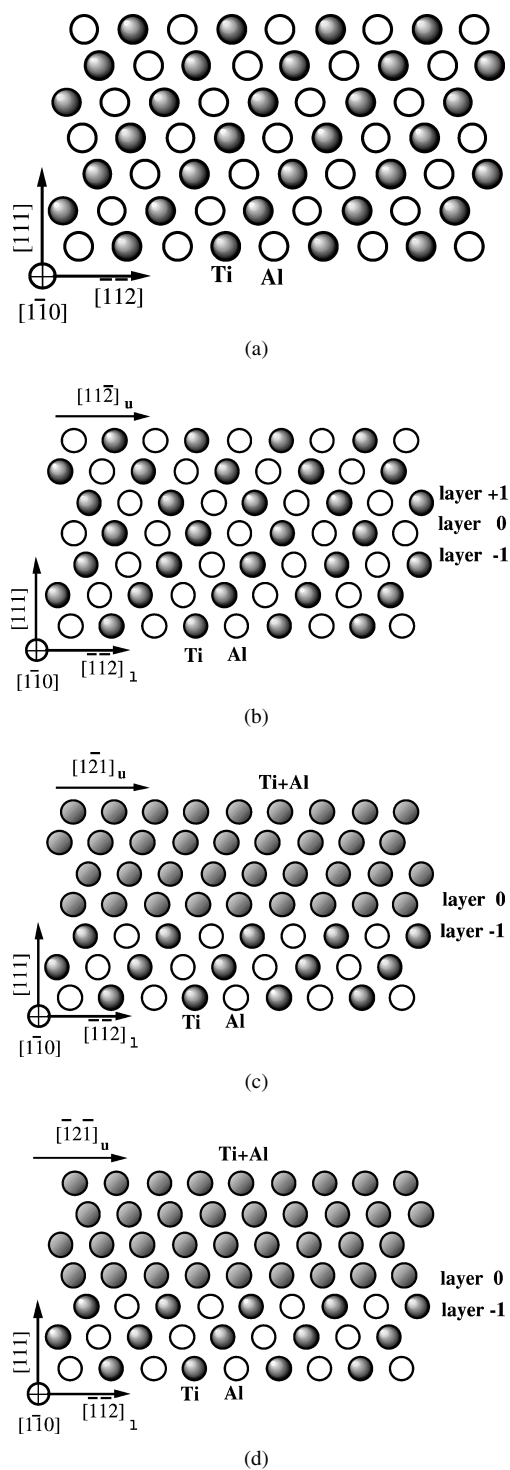
Figure 2. Atomic structure of the ideal L1$_0$ TiAl and the three $\gamma - \gamma$ interfaces in this structure depicted in the [$\bar{1}$10] projection. (a) Ideal L1$_0$ TiAl; (b) Ordinary twin; (c) Pseudotwin; (d) 120° rotational fault. Open circles represent Al, filled circles Ti and gray circles represent atomic rows of mixed composition.

period interfaces of this type. This was enabled by using the many-body central force potentials fitted such as to give $c/a = 1$ for the minimum energy structure (see Appendix).

3. Methods of Atomistic Modeling of Formation and Migration of Vacancies

3.1. Description of Atomic Interactions

In the present calculations the total energy was evaluated using the central-force Finnis-Sinclair type potentials [33] for binary alloys [34]. In this scheme the energy is written as

$$E = \sum_{i=1}^{N} \left[\frac{1}{2} \sum_{j \neq i} V_{S_i S_j}(r_{ij}) - \sqrt{\rho_i} \right] \qquad (1a)$$

where

$$\rho_i = \sum_{j \neq i} \Phi_{S_i S_j}(r_{ij}), \qquad (1b)$$

N is the total number of atoms in the system and both V and Φ are empirically fitted pair potentials; the second term in Eq. (1a) is the many-body term. The suffices i and j refer to individual atoms and S_i and S_j to the species of the atoms involved. The summation over j extends over those neighbors of the atom i for which r_{ij}, the separation of atoms i and j, is within the cut-off radii of these potentials.

For the Ti-Al system such potentials were originally developed in the context of atomistic studies of dislocations [35, 36]. Two sets of potentials were constructed for TiAl with the tetragonal L1$_0$ lattice. One reproduces exactly the lattice parameters c and a and thus the non-ideal c/a ratio, and the other leads to $c/a = 1$. As alluded to in the previous section the latter potentials were used in the present study. Both sets of potentials reproduce the cohesive energy and to a good approximation the elastic moduli. However, owing to the negative Cauchy pressures C$_{12}$-C$_{66}$ and C$_{13}$-C$_{44}$ the elastic moduli cannot be fitted exactly in this scheme [36]. Nevertheless, these potentials assure stability of the L1$_0$ ordering relative to disordering, stability of the L1$_0$ lattice with respect to the alternate structures with the same stoichiometry, B2 and B19, and mechanical stability with respect to some large homogeneous deformations [35–37]. Hence, it is reasonable to assume that calculations employing these potentials can reveal,

102   *Nomura and Vitek*

at least qualitatively, the role of lamellar interfaces in self-diffusion in TiAl. Details of the potentials used are presented in the Appendix.

3.2.   Technique of Atomistic Calculations

A finite block of the $L1_0$ lattice was first constructed geometrically. Since all the interfaces investigated are parallel to the (111) planes, external surfaces of this block are also parallel to these planes. The interfaces studied were then introduced into the middle of the block such that the bottom half of the block remained fixed while the upper half was rotated around the [111] axis by $n\pi/3$, where $n = 1, 2$, and 3, to create a pseudotwin, a $120°$ rotational fault and an ordered twin, respectively. In all cases the block consisted of twenty-six (111) layers the repeat cell of which was composed of sixty $\frac{1}{2}[1\bar{1}0] \times \frac{1}{2}[11\bar{2}]$ unit cells and contained 120 atoms; the total number of atoms in the repeat cell of the block was then 3120. The minimum energy structures of the interfaces studied were determined by relaxing all the atoms using a conjugate gradient method for energy minimization employing the DYNAMO code developed by Daw and co-workers in connection with the advancement of the embedded atom method [38–40].

In atomistic studies of vacancy formation the starting configurations were always the fully relaxed interfacial structures. Atoms were then removed at several different sites at and in the vicinity of the interface, and these configurations always relaxed using again a conjugate gradient method. The evaluation of the effective formation energies of the vacancies is described in more detail in the following section. Since this requires information on antisite defects, these were also analyzed using the same approach as in the case of vacancies.

When investigating vacancy migration we evaluated the migration energies employing the diffusional paths, summarized in Section 3.4, which were recently proposed in studies of bulk diffusion in TiAl by Mishin and co-workers [1, 2]. The calculations employed procedures used in earlier studies of vacancy migration in grain boundaries [41–44]. Starting with the fully relaxed structure of a vacancy, the migration path was always defined by movement of an atom located near the vacancy. This atom was then moved by small steps along this path. At each step the migrating atom was allowed to relax in the plane perpendicular to the migration path while all the other atoms were allowed to relax fully in all directions. The vacancy migration

energy, E_V^m, was then identified with the maximum energy attained during this process, relative to the initial state.

3.3.   Formation of Vacancies

In elemental solids the equilibrium concentration of vacancies at a temperature T is given as

$$c_V = c_0 \exp\left(-\frac{E_V^f}{k_B T}\right) \qquad (2)$$

where E_V^f is the vacancy formation energy, c_0 the pre-exponential factor of the order one, related to vibrational entropy, and k_B the Boltzmann constant. In alloys the situation is more complex. First, there is no unique definition of the cohesive energy of individual species but only the cohesive energy per atom of the alloy, E_{coh}, has a physical meaning. Secondly, formation of vacancies is necessarily accompanied by formation of antisite defects if stoichiometry is not to change. These problems have recently been analyzed in detail in references [2, 45–47] and here we only briefly summarize those results needed in the present study.

In the context of atomistic studies of vacancies and antisite defects the important concept is the "raw" energy of such defects. This is defined as the total change of the energy of the block used in the simulation when the defect was introduced, and the block relaxed, while the number of lattice sites was kept fixed. Thus the "raw" energies of vacancies on sites A and B, $E_{V_A}^*$ and $E_{V_B}^*$, respectively, are the differences of energies of the block with and without the corresponding vacancies. The "raw" energies of antisite defects, $E_{A\rightarrow B}^*$, corresponding to replacing a B atom by the A atom, and $E_{B\rightarrow A}^*$, corresponding to replacing an A atom by the B atom, are evaluated analogously. As explained in [2, 47] the "raw" energies must not be confused with the formation energies of the corresponding point defects. However, they are quantities that can be easily evaluated in atomistic studies and relate, via statistical mechanics considerations, to the effective formation energies of point defects that determine their concentrations by equations analogous to (2) [2, 47]. In a stoichiometric binary $A_n B_m$ alloy the effective vacancy formation energies at sites A and B, respectively, are

$$E_{V_A}^{eff} = E_{V_A}^* + E_{coh} + \frac{b}{2}(E_{A\rightarrow B}^* - E_{B\rightarrow A}^*) \quad (3a)$$

$$E_{V_B}^{eff} = E_{V_B}^* + E_{coh} + \frac{a}{2}(E_{B\rightarrow A}^* - E_{A\rightarrow B}^*) \quad (3b)$$

where $a = n/(m + n)$ and $b = m/(m + n)$, and the effective formation energies of antisite defects are

$$E_{A \to B}^{eff} = E_{B \to A}^{eff} = \frac{1}{2}(E_{B \to A}^* + E_{A \to B}^*) \qquad (3c)$$

In an $A_n B_m$ alloy with the surplus of A the corresponding effective formation energies are

$$E_{V_A}^{eff} = E_{V_A}^* + E_{coh} + bE_{A \to B}^* \qquad (4a)$$

$$E_{V_B}^{eff} = E_{V_B}^* + E_{coh} - aE_{A \to B}^* \qquad (4b)$$

$$E_{A \to B}^{eff} = 0; \quad E_{B \to A}^{eff} = E_{B \to A}^* + E_{A \to B}^* \qquad (4c)$$

3.4. Migration of Vacancies and Diffusion

A vacancy moving randomly through an ordered structure would generally involve jumps from one sublattice to the other and this would lead to gradually increasing disorder. Therefore, in thermodynamic equilibrium vacancy jumps must be correlated with one another and occur in a way that preserves the order [2]. For the bulk TiAl such jumps have been identified in Refs. [1, 2]. In this study we investigate only those paths that are parallel to (111) planes and enable diffusion in $\gamma - \gamma$ interfaces. The jumps out and back into the interface, with a component parallel to the interface, were also considered but they were generally found to be less probable.

The simplest jumps that maintain the order are movements of vacancies along one of the sublattices. In TiAl the nearest neighbor jumps of this type, marked in the following NN, are in the $[\bar{1}10]$ direction (cf. Fig. 1). The jump along the Ti sublattice in the $[\bar{1}10]$ direction is shown schematically in Fig. 3; the same type of jump may occur on the Al sublattice. Since the $[\bar{1}10]$ direction is parallel to the (111) plane, these jumps can also be considered as possible diffusional steps along $\gamma - \gamma$ interfaces.

Another possibility is chains of transitions in which the atomic order is intermittently destroyed but it is fully restored at the end of each chain. Two such mechanisms are considered in this study. The first is a three-jump cycle, proposed in [1, 2] and marked in the following as 3JC. The other is the antistructural bridge mechanism, first proposed in [48], and marked in the following as ASB. In the 3JC, shown schematically in Fig. 3 (see also Fig. 22 of [2]), a vacancy on the Al sublattice makes first a jump to the Ti sublattice. At this point an antisite defect is formed temporarily. Then another jump along the Ti sublattice takes place
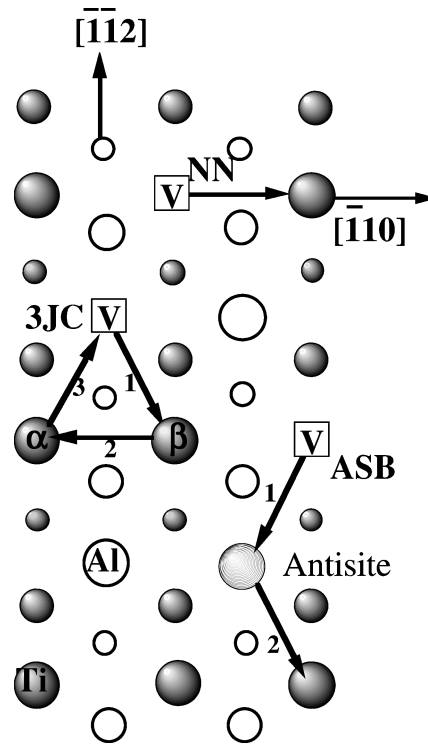
Figure 3. Structure of the three successive (111) planes, distinguished by sizes of the circles representing the atoms; open circles represent Al and filled circles Ti. Three mechanisms of the migration of vacancies in the (111) planes, NN, 3JC and ASB, are depicted by arrows representing the sequences of the vacancy jumps.

and finally the vacancy returns to the original position. As a result two atoms on the Ti sublattice, marked α and β in Fig. 3, exchange positions. As discussed in [2], this mechanism leads to the transport of Ti atoms in combination with diffusion of vacancies on the Al sublattice and the two mechanisms are linked through the jump correlation factor. The resulting movement of Ti atoms is in the $[\bar{1}10]$ direction that lies in the (111) plane and thus this mechanism may also operate in $\gamma - \gamma$ interfaces. Analogously, a vacancy on the Ti sublattice may induce transport of atoms on the Al sublattice.

The ASB mechanism, in contrast to the 3JC mechanism, requires not only pre-existing vacancies but also antisites and consists of two nearest neighbor jumps of the vacancy, resulting in NN type displacements of two atoms of the same species. Two alternatives, ASB1 and ASB2, have been considered in [2] (see Fig. 24(b) of [2]). In the former case the vacancy and the antisite belong to the same sublattice and in the latter case to different sublattices. However, in ASB1 the movement of the vacancy is of the same type as in the NN

jump and this jump is likely to dominate over the ASB1 jump; this has, indeed, been corroborated by calculations in [2]. Hence, in this paper we only consider the mechanism ASB2 and call it ASB. It is shown schematically in Fig. 3 where it involves one vacancy on the Ti sublattice and one antisite on the Al sublattice and consists of two nearest neighbor jumps of the vacancy resulting in displacements of Ti atoms. Analogously, a vacancy on the Al sublattice, together with the antisite on the Ti sublattice, may induce transport of Al atoms. This mechanism leads to atomic transport along $\langle 112 \rangle$ directions and thus parallel to $\{111\}$ planes.

The diffusion coefficient, D, associated with a given mechanism can be written approximately as $D \propto c_1 \cdot c_2 \cdot \ldots \exp(-E^m / k_B T)$, where c_i are concentrations of defects needed in the migration process and E^m is the corresponding migration energy evaluated as discussed in Section 3.2. Since $c_i \propto \exp(-E_i^f / k_B T)$, where E_i^f is the effective formation energy of the defect i, we can write

$$D = D_0 \exp\left(-\frac{Q^{\text{eff}}}{k_B T}\right). \quad (5a)$$

Here D_0 is a prefactor and

$$Q^{\text{eff}} = \sum_i E_i^f + E^m \quad (5b)$$

where the summation extends over the point defects needed for a given mechanism. For the NN and 3JC mechanisms the only defects involved are the corresponding vacancies and thus in these two cases $Q^{\text{eff}} = E_V^{\text{eff}} + E_V^m$. However, it should be noticed that the diffusing species and the vacancies belong to the same sublattice in the case of the NN mechanism and to different sublattices in the case of the 3JC mechanism. For the ASB mechanism considered, $Q^{\text{eff}} = E_V^{\text{eff}} + E_{\text{Antisite}}^m + E_V^m$. When the diffusing species are from the sublattice A the vacancy is from the same sublattice but the antisite belongs to the sublattice B and vice versa. However, as pointed out in [2], Eq. (5a) is only a rough approximation in which the value of D_0 is assumed to be the same for all the mechanisms while substantial differences may arise due to entropy factors, geometry and jump correlations. Nevertheless, this approximation provides a simple method for the assessment of the importance of various mechanisms, though a more detailed analysis requires more rigorous methods, such as kinetic Monte Carlo (see for example [49]).

Table 1. Effective formation energies (in eV) of Ti and Al vacancies and antisites in the bulk TiAl.

	$E_{V_n}^{\text{eff}}$	$E_{V_{Al}}^{\text{eff}}$	$E_{\text{Antisite}}^{\text{eff}}$
Present study	1.40	1.63	0.44
Ref. [2]	1.15	1.41	0.44
Ref. [50]	1.95	2.46	0.72
Ref. [51]	1.59	1.99	0.60
Ref. [52]	1.05	1.28	0.82

4. Results

4.1. Bulk TiAl

The calculations outlined above were first carried out for the bulk TiAl in the $L1_0$ structure. The effective vacancy formation energies evaluated using Eqs. (3a) and (b) are summarized in Table 1 ($a = b = 1/2$ for TiAl). The effective formation energies of antisite defects, needed in the analysis of the ASB mechanism, are also presented. For comparison we include results of Mishin and Herzig [2], obtained using the EAM, results of *ab initio*, local density functional theory calculations [50, 51], as well as results of recent calculations employing the tight-binding based bond-order potentials [52]. The main difference between the description of interatomic forces used in this study, as well as in Ref. [2], and calculations employing *ab initio* methods and bond-order potentials is that in the latter case the possible directional character of bonding is properly accounted for. This covalent type bonding arises in Ti–Al alloys due to d electrons associated with Ti and p electrons associated with Al. While the absolute values of the effective formation energies calculated by different methods vary up to 50%, they are of the same order of magnitude and display the same trends.[1] In particular, in all cases it is predicted that there will be a higher concentration of Ti vacancies than Al vacancies and disorder will occur via formation of antisites rather than structural vacancies. The latter is consistent with experimental observations [53–55]. This suggests that the directional bonding does not play a determining role in qualitative analyses of point defects, presumably owing to their nearly spherical symmetry, and central force description of atomic interactions is adequate.

The migration energies, E_V^m, and related values of Q^{eff} for the migration mechanisms discussed in Section 3.4 , are summarized in Table 2. For comparison we also include results of Ref. [2]. It is seen that

Table 2. Migration energies of Ti and Al vacancies and effective activation energies (in eV) for diffusion of Ti and Al by different mechanisms in the bulk of TiAl.

Mechanisms	E_V^m			Q^{eff}		
	NN	3JC	ASB	NN	3JC	ASB
Present study						
Titanium	1.07	1.40	0.72	2.47	2.90	2.56
Aluminum	0.91	1.27	0.57	2.54	2.80	2.64
Ref. [2]						
Titanium	1.45	1.82	0.71	2.60	2.88	2.30
Aluminum	1.23	1.47	1.32	2.64	2.97	3.17

both calculations display similar trends in migration mechanisms. The 3JC mechanism of the diffusion is the most difficult mechanism for both Ti and Al vacancies. The values of Q^{eff} for the NN and ASB mechanisms are in the present study very similar so that these two mechanism may be expected to contribute practically equally to the diffusion of both Ti and Al. A similar result has been found in [2] for Ti but the ASB is the most difficult mechanism for Al. The reason for this difference is not obvious and could only be understood after a detailed comparison of the two studies.

4.2. Interfaces with Stoichiometric Composition

Since the goal of this study is investigation of the diffusion at $\gamma-\gamma$ interfaces found in the lamellar TiAl based alloys, calculations similar to those performed for the bulk have been made for the three types of $\gamma-\gamma$ interfaces defined in Section 2. The point defects, vacancies and antisites, were considered in two layers adjacent to the interfaces, marked 0 and -1 in Fig. 2(b)–(d).

Limited calculations were also made for layers further away from the interfaces but the corresponding formation energies were found to be practically the same as in the bulk. In the case of the ordinary twin there is only one non-equivalent Ti and one non-equivalent Al site per layer but in the case of the pseudotwin and the rotational fault there are two distinct Ti and Al sites per layer.

The very important feature of interfacial vacancies, found in the calculations, is that relaxations of atoms in their vicinity are not more significant than in the bulk. Hence, the vacancies at the interfaces are as localized as in the bulk and therefore the interfacial diffusion can be considered as mediated by vacancies via mechanisms similar to those identified in the bulk. The effective formation energies of vacancies and antisites at distinct lattice sites in the vicinity of the three interfaces studied are summarized in Table 3; these energies were again calculated using Eqs. (3a) and (b). They are generally lower than in the bulk, albeit not greatly, and thus vacancies are weakly attracted to all three $\gamma-\gamma$ interfaces considered. It is notable that for a given interface they do not differ significantly for different non-equivalent sites. Moreover, it is interesting that the effective formation energies of vacancies are the lowest at the ordinary twin, 18–20% lower than in the bulk, while they are only 9–12% lower than in the bulk for the pseudotwin and 5–8% lower for the rotational fault.

The migration energies, E_V^m, and related values of Q^{eff} for the three migration mechanisms considered, are summarized in Table 4. In the case of two non-equivalent vacancy sites, the site with lower effective formation energy was always used when evaluating the migration energies. Comparison with Table 2 shows that, in general, the migration along $\gamma-\gamma$ interfaces is somewhat easier than in the bulk, albeit not remarkably.

Table 3. Effective formation energies of Ti and Al vacancies and antisites (in eV) in two layers of $\gamma-\gamma$ stoichiometric interfaces in TiAl. Two different values correspond to two distinct sites in the layer.

Type of interface	Layer number	$E_{V_n}^{\text{eff}}$	$E_{V_{Al}}^{\text{eff}}$	$E_{\text{Antisite}}^{\text{eff}}$
Ordinary twin	0	1.15	1.33	0.43
	-1	1.14	1.33	0.43
Pseudotwin	0	1.28 and 1.39	1.43 and 1.57	0.44 and 0.18
	-1	1.27 and 1.39	1.43 and 1.57	0.44 and 0.18
Rotational fault	0	1.32 and 1.34	1.50 and 1.51	0.31 and 0.30
	-1	1.33 and 1.35	1.50 and 1.51	0.31 and 0.30

Table 4. Migration energies of Ti and Al vacancies and effective activation energies (in eV) for Ti and Al diffusion by different mechanism in stoichiometric $\gamma-\gamma$ interfaces.

	Layer number	E_V^m			Q^{eff}		
		NN	3JC	ASB	NN	3JC	ASB
		Ordinary twin					
Titanium	0	0.76	1.06	0.66	1.91	2.29	2.24
	−1	0.76	1.06	0.66	1.90	2.24	2.23
Aluminum	0	0.57	0.96	0.40	1.90	2.21	2.16
	−1	0.58	0.91	0.50	1.91	2.20	2.26
		Pseudotwin					
Titanium	0	0.93	1.04	0.59	2.21	2.54	2.05
	−1	1.03	1.17	0.83	2.30	2.47	2.28
Aluminum	0	0.81	1.11	0.75	2.24	2.32	2.36
	−1	0.95	1.04	0.60	2.38	2.44	2.21
		Rotational fault					
Titanium	0	0.96	1.07	0.66	2.28	2.50	2.28
	−1	0.90	1.17	0.76	2.23	2.54	2.39
Aluminum	0	0.86	1.00	0.60	2.36	2.39	2.40
	−1	0.95	1.04	0.63	2.45	2.50	2.43

In most cases E_V^m and Q^{eff} are the lowest for the NN mechanism and highest for the 3JC mechanism, similarly as in the bulk. However, while in the bulk the diffusion of Al is in most cases more difficult than the diffusion of Ti, in the interfaces this difference is less conspicuous. It is interesting that, similarly as the formation of vacancies, the diffusion is easiest in the ordinary twin, in particular via the NN mechanism. This is contrary to the notion that since the structure of this interface is closer to that of the bulk than the structure of the other two interfaces, its diffusion characteristics should be closest to the bulk.

4.3. Interfaces with Surplus of Titanium

As mentioned above, the recent Monte Carlo study of $\gamma-\gamma$ interfaces in Ti-rich alloys suggests that a very thin layer with composition close to the DO_{19} Ti_3Al forms at $120°$ rotational faults and pseudotwins [28]. Hence, in this study we investigated formation and migration of vacancies in these two interfaces when the central layer, i.e. layer 0 in Fig. 1(c) and (d), has the composition and structure of Ti_3Al while all the other layers possess the stoichiometric TiAl composition. The effective formation energies of vacancies and antisites in such interfaces are summarized in Table 5. These

Table 5. Effective formation energies of Ti and Al vacancies and Al → Ti antisites (in eV) in two layers of $\gamma-\gamma$ interfaces with segregated Ti. Layer 0 has the Ti_3Al composition and structure. Note that in this case $E_{Ti \to Al}^{eff} \approx 0$.

Type of interface	Layer number	$E_{V_n}^{eff}$	$E_{V_{Al}}^{eff}$	$E_{Al \to Ti}^{eff}$
Pseudotwin	+1	1.38	1.55	0.31
	0	1.66	1.74	0.05
	−1	1.33	1.48	0.18
Rotational fault	+1	1.56	1.56	0.31
	0	1.84	1.70	0.31
	−1	1.39	1.56	0.31

energies were calculated using Eqs. (4a)–(c) since Ti is in surplus in this region. However, use of these relations implies several approximations, most significantly that E_{coh} does not depend on the concentration of Ti and that Ti → Al antisites do not interact in spite of their high concentration. Comparison with Table 3 shows that formation of vacancies in non-stoichiometric interfaces is generally more difficult and in the layer 0, which contains surplus of Ti, even more difficult than in the bulk. In contrast, formation of antisite defects is easier than in both the bulk and stoichiometric interfaces suggesting that disordering is relatively easy in the vicinity of the layer with the surplus of Ti. Such

Table 6. Migration energies of Ti and Al vacancies and effective activation energies (in eV) for Ti and Al diffusion by different mechanisms in $\gamma-\gamma$ interfaces with segregated Ti. Layer 0 has the Ti_3Al composition and structure.

	Layer number	E_V^m			Q^{eff}		
		NN	3JC	ASB	NN	3JC	ASB
			Pseudotwin				
Titanium	+1	1.02	1.27	0.83	2.40	2.71	2.52
	0	0.67	–	0.63	2.33	2.32	2.34
	−1	0.99	0.94	0.79	2.32	2.47	2.30
Aluminum	+1	0.93	1.16	0.57	2.48	2.65	2.12
	0	–	0.58	0.58	–	–	2.32
	−1	0.72	0.99	0.77	2.20	2.27	2.25
			Rotational fault				
	+1	1.07	1.29	0.81	2.63	2.67	2.68
Titanium	0	0.78	–	0.56	2.62	2.72	2.50
	−1	1.01	1.26	0.83	2.40	2.65	2.53
	+1	0.96	1.11	0.58	2.52	2.85	2.14
Aluminum	0	–	1.02	0.79	–	–	2.49
	−1	0.92	1.09	0.60	2.48	2.65	2.16

local disordering was also revealed in the Monte Carlo calculations [28].

The migration energies, E_V^m, and related values of Q^{eff} for the three migration mechanisms considered, are summarized in Table 6. It should be noted that owing to higher concentration of Ti in the layer 0 the NN migration jumps of Al vacancies and 3JC jumps of Ti vacancies can not occur in this layer. Comparison of Tables 6 and 4 shows that on average there is no significant difference in diffusional propensity between stoichiometric interfaces and interfaces rich in titanium. This is so in spite of the fact that formation of vacancies is more difficult in interfaces with the surplus of Ti. The reason is that this is compensated by easier migration of vacancies in such interfaces that leads to very similar overall diffusional behavior.

5. Discussion

The first finding of the atomistic studies presented in this paper is that the effective formation energies of vacancies at $\gamma-\gamma$ interfaces in TiAl are generally somewhat lower than in the bulk. The lowest effective formation energies for both Ti and Al vacancies have been found in the ordinary twin where they are about 20% below those in the bulk. In the pseudotwin and 120°

rotational fault they are about 10% lower. This is in contrast with grain boundaries where the vacancy formation energies may be factor of two or more lower than in the bulk [1, 19–21, 41–43]. The main structural difference is that in grain boundaries there is very significant local relaxation near vacancies that may lead to their delocalization [49, 56], while in $\gamma-\gamma$ interfaces vacancies are practically as localized as in the bulk. Such localization is, of course, common in twin boundaries [44, 57, 58] and it is the main reason why vacancy formation energies in such boundaries are also not too different from those in the bulk.

Similarly, the migration energies for the three mechanisms studied are lower in $\gamma-\gamma$ interfaces than in the bulk, again with the lowest values for the ordinary twin. The corresponding effective activation energies for diffusion are on average about 15% lower than in the bulk so that the diffusivity along these interfaces is higher than in the bulk, albeit not drastically as it may be in the case of grain boundaries [19–21, 41–43]. Furthermore, the effective activation energies are very similar in all three types of interfaces and not very different for Ti and Al, respectively. Hence, self-diffusion of both Ti and Al can be expected to be enhanced relative to the bulk in all $\gamma-\gamma$ interfaces and be similar for both elements.

An interesting finding is that the surplus of Ti at the pseudotwin and 120° rotational fault, which may

108   *Nomura and Vitek*

occur due to segregation [27, 28], affects the diffusivity in these interfaces only marginally. In the present study the titanium surplus was modeled as a layer with the Ti_3Al DO_{19}-type structure at these interfaces, as indicated by Monte Carlo calculations of Ti segregation to lamellar interfaces when there is a surplus of Ti in the bulk [28]. It could be expected that this large structural and stoichiometric difference at the interface affects significantly both the formation and migration of vacancies and thus the interfacial diffusion coefficient. Nonetheless, as seen in Table 6, the effective activation energies for diffusion differ only marginally from those presented in Table 4 for the stoichiometric case. The reason is that the controlling step of diffusion is the vacancy formation and migration in the layer adjacent to the Ti rich layer. Hence, the present study suggests that segregation of Ti to some lamellar boundaries will not affect their diffusional properties very significantly. However, a bigger effect of the surplus of titanium on interfacial diffusion might be found if the directional bonding arising from the Ti d-electrons were taken into account in the calculations. Consequently, the present results showing a small effect of Ti segregation, which have been obtained using central-force potentials, should not be taken as definite.

Appendix A: Many-Body Central-Force Finnis-Sinclair Potentials for TiAl

The functional forms of the potentials entering Eqs. (1a) and (b) are:

$$V_{AA}(r_{ij}) = \sum_{k=1}^{6} a_k (r_k - r_{ij})^3 H(r_k - r_{ij})$$

$$\Phi_{AA}(r_{ij}) = \sum_{k=1}^{2} A_k (R_k - r_{ij})^3 H(r_k - r_{ij}),$$

(A.1)

where A represents either Ti or Al, and

$$V_{TiAl}(r_{ij}) = \sum_{k=1}^{4} a_k (r_k - r_{ij})^3 H(r_k - r_{ij})$$

$$\Phi_{TiAl} = \sqrt{\Phi_{TiTi}\Phi_{AlAl}},$$

(A.2)

where $H(x)$ is the Heaviside step function and the corresponding parameters a_k, A_k, r_k and R_k are summarized in Table A1. The values of r_1 and R_1 represent cut-off radii of the corresponding potentials.

Table A.1. Parameters of the V_{TiTi}, Φ_{TiTi}, V_{AlAl}, Φ_{AlAl} and V_{TiAl} potentials that lead to $a = c = 4.0246$ Å and the ratio $c/a = 1$. The radii r_i and R_i are in Å and coefficients a_i and A_i in eV/Å^3.

	Ti	Al	Ti–Al
a_1	−0.892173390625	0.485497090961	0.0756562605
a_2	1.261493718750	−1.122148021598	−0.1639193100
a_3	−0.340022937500	2.107197460791	0.3990835860
a_4	−0.162444984375	−1.619069618174	0.2034540000
a_5	1.164297312500	0.443144698322	
a_6	0.561266250000	0.301001333565	
A_1	0.621811359375	0.289298308255	
A_2	−0.610332890625	0.074641404172	
r_1	4.88	4.9616175	4.70
r_2	4.80	4.7793540	4.30
r_3	4.48	4.4148270	3.70
r_4	3.80	4.2528150	3.25
r_5	3.20	3.6452700	
r_6	2.828428	3.0665096	
R_1	4.88	4.860360	
R_2	4.16	3.766779	

Note

1. The higher values of effective formation energies found in *ab initio* calculations [50, 51] may be a consequence of incomplete structural relaxations.

References

1. C. Herzig, T. Przeorski, and Y. Mishin, Intermetallics **7**, 389 (1999).
2. Y. Mishin and C. Herzig, Acta Mater. **48**, 589 (2000).
3. J.H. Westbrook and R.L. Fleischer, editors, *Intermetallic Compounds-Principles and Practice* (John Wiley, New York, 1995).
4. J.H. Westbrook, MRS Bull **21**, 37 (1996).
5. N.S. Stoloff, C.T. Liu, and S.C. Deevi, Intermetallics **8**, 1313 (2000).
6. M. Yamaguchi, H. Inui, and K. Ito, Acta Mater. **48**, 307 (2000).
7. F.R.N. Nabarro, Intermetallics **8**, 979 (2000).
8. H. Inui, M.H. Oh, A. Nakamura, and M. Yamaguchi, Acta Metall. Mater. **40**, 3095 (1992).

9. Y.-W. Kim, J. Metals **46**, 30 (1994).

10. M. Yamaguchi, H. Inui, K. Kishida, M. Matsumoro, and Y. Shirai, in *High-Temperature Ordered Intermetallic Alloys VI*, edited by J. Horton, I. Baker, S. Hanada, R.D. Noebe, and D. Schwartz, vol. 364 (Materials Research Society, Pittsburgh, 1995), p. 3.

11. M. Yamaguchi, H. Inui, S. Yokoshima, K. Kishida, and D.R. Johnson, Mat. Sci. Eng. A **213**, 25 (1996).

12. D.M. Dimiduk, Mat. Sci. Eng. A **263**, 281 (1999).

13. T. Tetsui, Curr Opin Solid State Mat. Sci. **4**, 243 (1999).

14. W. Dowling, W. Donlon, and J. Allison, in *High-Temperature Ordered Intermetallic Alloys VI*, edited by J.A. Horton, I. Baker, S. Hanada, R.D. Noebe, and D.S. Schwartz, vol. 364 (Materials Research Society, Pittsburgh, 1999), p. 757.

15. E.A. Loria, Intermetallics **8**, 1339 (2000).

16. E.A. Loria, Intermetallics **9**, 997 (2001).

17. D.M. Dimiduk, T.A. Parthasarathy, and P. M. Hazzledine, Intermetallics **9**, 875 (2001).

18. Y. Mishin and C. Herzig, Mat. Sci. Eng. A **260**, 55 (1999).

19. R.W. Balluffi, Metall. Trans. A **13**, 2069 (1982).

20. N.L. Peterson, Int. Met. Rev. **28**, 65 (1983).

21. R.W. Balluffi, in *Diffusion in Crystalline Solids*, edited by G.E. Murch and A.S. Nowick (Academic Press, Orlando, 1984), p. 319.

22. M.A. Grinfeld, in *Defect-Interface Interactions*, edited by E.P. Kvam, A.H. King, M.J. Mills, S.T.D., and V. Vitek, vol. 319 (Materials Research Society, Pittsburgh, 1994), p. 405.

23. I. Kaur, Y. Mishin, and W. Gust, *Fundamentals of Grain and Interface Boundary Diffusion* (John Wiley, Chichester, 1995).

24. Y. Mishin, C. Herzig, J. Bernardini, and W. Gust, Int. Mater. Rev. **42**, 155 (1997).

25. D.S. Schwartz and S.M.L. Sastry, Scripta Metall. **23**, 1621 (1989).

26. H. Inui, M.H. Oh, A. Nakamura, and M. Yamaguchi, Philos. Mag. A **66**, 539 (1992).

27. H. Inui, K. Kishida, M. Kobayashi, M. Yamaguchi, M. Kawasaki, and K. Ibe, Philos. Mag. A **74**, 451 (1996).

28. K. Ito and V. Vitek, Acta Mater. **46**, 5435 (1998).

29. C.R. Feng, D.J. Michel, and C.R. Crowe, Scripta Metall. **22**, 1481 (1988).

30. C. McCullough, J.J. Valencia, H. Mateous, C.G. Levi, R. Mehrabian, and K.A. Rhyne, Scripta Metall. **22**, 1131 (1988).

31. W.B. Pearson, *Handbook of Lattice Spacings and Structures of Metals and Alloys* (Pergamon Press, Oxford, 1967).

32. B.K. Kad and P.M. Hazzledine, Philos. Mag. Lett. **66**, 133 (1992).

33. M.W. Finnis and J.E. Sinclair, Philos. Mag. A **50**, 45 (1984).

34. G.J. Ackland and V. Vitek, Phys. Rev. B **41**, 10324 (1990).

35. A. Girshick and V. Vitek, in *High-Temperature Ordered Intermetallic Alloys VI*, edited by J. Horton, I. Baker, S. Hanada, R. D. Noebe, and D. Schwartz, vol. 364 (Materials Research Society, Pittsburgh, 1995), p. 145.

36. V. Vitek, A. Girshick, R. Siegl, H. Inui, and M. Yamaguchi, in *Properties of Complex Inorganic Solids*, edited by A. Gonis, A.-M. Meike, and P.E.A. Turchi (Plenum Press, New York, 1997), p. 355.

37. V. Paidar, L.G. Wang, M. Sob, and V. Vitek, Modelling and Simulation in Mat. Sci. Eng. **7**, 369 (1999).

38. M.S. Daw and M.I. Baskes, Phys. Rev. Lett. **50**, 1285 (1983).

39. M.S. Daw, in *Atomistic Simulations of Materials: Beyond Pair Potentials*, edited by V. Vitek and D. Srolovitz (Plenum Press, New York, 1989), p. 181.

40. M.S. Daw, S.M. Foiles, and M.I. Baskes, Mater Sci Rep **9**, 251 (1993).

41. M. Nomura, S.-Y. Lee, and J. B. Adams, J. Mater. Res. **6**, 1 (1991).

42. M. Nomura and J.B. Adams, J. Mater. Res. **7**, 3202 (1992).

43. D. Farkas, J. Phys.: Condens. Matter **12**, R497 (2000).

44. J.R. Fernandez, A.M. Monti, R.C. Pasianot, and V. Vitek, Philos. Mag. A **80**, 1349 (2000).

45. Y. Mishin and D. Farkas, Philos. Mag. A **75**, 169 (1997).

46. Y. Mishin and D. Farkas, Philos. Mag. A **75**, 187 (1997).

47. M. Hagen and M.W. Finnis, Philos. Mag. A **77**, 447 (1998).

48. C.R. Kao and Y.A. Chang, Intermetallics **1**, 237 (1993).

49. M.R. Sorensen, Y. Mishin, and A.F. Voter, Phys. Rev. B **62**, 3658 (2000).

50. C.L. Fu and M.H. Yoo, Phys. Rev. Lett. **62**, 159 (1990).

51. C. Woodward, S. Kajihara, and L.H. Yang, Phys. Rev. B **57**, 13459 (1998).

52. S. Znam, PhD Thesis, University of Pennsylvania, 2001.

53. Y. Shirai and M. Yamaguchi, Mat. Sci. Eng. A **152**, 173 (1992).

54. U. Brossmann, R. Würschum, K. Badura, and H.-E. Schaefer, Phys. Rev. B **49**, 6457 (1994).

55. M. Yamaguchi and Y. Shirai, in *Physical Metallurgy and Processing of Intermetallic Compounds*, edited by N.S. Stoloff and V.K. Sikka (Chapman and Hall, New York, 1996), p. 3.

56. V. Vitek, Y. Minonishi, and G.J. Wang, J. Phys. France **46**, C4 (1985).

57. B.A. Faridi and A.G. Crocker, Philos. Mag. A **41**, 137 (1980).

58. N. DeDiego and D.J. Bacon, Philos. Mag. A **63**, 873 (1991).